

# Differentiation of pancreatic cysts with optical coherence tomography (OCT) imaging: an *ex vivo* pilot study

Nicusor Iftimia,<sup>1,6,\*</sup> Sevdener Cizginer,<sup>2,6</sup> Vikram Deshpande,<sup>3</sup> Martha Pitman,<sup>3</sup> Servet Tatli,<sup>4</sup> Nicolae-Adrian Iftimia,<sup>5</sup> Daniel X Hammer,<sup>1</sup> Mircea Mujat,<sup>1</sup> Teoman Ustun,<sup>1</sup> R. Daniel Ferguson,<sup>1</sup> and William R. Brugge<sup>2</sup>

<sup>1</sup>Physical Sciences, Inc., Andover, Massachusetts, USA

<sup>2</sup>Massachusetts General Hospital, Gastrointestinal Unit, Massachusetts, USA

<sup>3</sup>Massachusetts General Hospital, Department of Pathology, Massachusetts, USA

<sup>4</sup>Brigham and Women's Hospital, Department of Radiology, Massachusetts, USA

<sup>5</sup>Brandeis University, Waltham, Massachusetts, USA

<sup>6</sup>Equal contribution

\*iftimia@psicorp.com

**Abstract:** We demonstrate for the first time that optical coherence tomography (OCT) imaging can reliably distinguish between morphologic features of low risk pancreatic cysts (i.e., pseudocysts and serous cystadenomas) and high risk pancreatic cysts (i.e., mucinous cystic neoplasms and intraductal papillary mucinous neoplasms). In our study fresh pancreatotomy specimens (66) from patients with cystic lesions undergoing surgery were acquired and examined with OCT. A training set of 20 pathology-OCT correlated tissue specimens were used to develop criteria for differentiating between low and high risk cystic lesions. A separate (validation) set of 46 specimens were used to test the OCT criteria by three clinicians, blinded to histopathology findings. Histology was finally used as a 'gold' standard for testing OCT findings. OCT was able to reveal specific morphologic features of pancreatic cysts and thus to differentiate between low-risk and high-risk cysts with over 95% sensitivity and specificity. This pilot study suggests that OCT could be used by clinicians in the future to more reliably differentiate between benign and potentially malignant pancreatic cysts. However, *in vivo* use of OCT requires a probe that has to fit the bore of the pancreas biopsy needle. Therefore, we have developed such probes and planned to start an *in vivo* pilot study within the very near future.

© 2011 Optical Society of America

**OCIS codes:** (170.0170) Medical optics and biotechnology; (170.4580) Optical diagnostics for medicine; (170.4500) Optical coherence tomography; (170.6935) Tissue characterization.

---

## References and links

1. W. R. Brugge, G. Y. Lauwers, D. Sahani, C. Fernandez-del Castillo, and A. L. Warshaw, "Cystic neoplasms of the pancreas," *N. Engl. J. Med.* **351**(12), 1218–1226 (2004).
2. K. S. Lee, A. Sekhar, N. M. Rofsky, and I. Pedrosa, "Prevalence of incidental pancreatic cysts in the adult population on MR imaging," *Am. J. Gastroenterol.* **105**(9), 2079–2084 (2010).
3. D. V. Sahani, J. C. Miller, C. Fernández del Castillo, W. R. Brugge, J. H. Thrall, and S. I. Lee, "Cystic pancreatic lesions: classification and management," *J. Am. Coll. Radiol.* **6**(5), 376–380 (2009).
4. J. A. Wargo, C. Fernandez-del-Castillo, and A. L. Warshaw, "Management of pancreatic serous cystadenomas," *Adv. Surg.* **43**(1), 23–34 (2009).
5. M. P. Federle and K. M. McGrath, "Cystic neoplasms of the pancreas," *Gastroenterol. Clin. North Am.* **36**(2), 365–376, ix (2007).
6. R. H. Hruban, M. B. Pitman, and D. S. Klimstra, *Tumors of the Pancreas*, AFIP Atlas of Tumor Pathology; 4th Series Fascicle 6 (American Registry of Pathology, 2007).

7. A. J. Megibow, F. P. Lombardo, A. Guarise, G. Carbognin, J. Scholes, N. M. Rofsky, M. Macari, E. J. Balthazar, and C. Procacci, "Cystic pancreatic masses: cross-sectional imaging observations and serial follow-up," *Abdom. Imaging* **26**(6), 640–647 (2001).
8. C. Procacci, C. Biasiutti, G. Carbognin, S. Accordini, E. Bicego, A. Guarise, E. Spoto, I. A. Andreis, R. De Marco, and A. J. Megibow, "Characterization of cystic tumors of the pancreas: CT accuracy," *J. Comput. Assist. Tomogr.* **23**(6), 906–912 (1999).
9. N. A. Ahmad, M. L. Kochman, C. Brensinger, W. R. Brugge, D. O. Faigel, F. G. Gress, M. B. Kimmey, N. J. Nickl, T. J. Savides, M. B. Wallace, M. J. Wiersema, and G. G. Ginsberg, "Interobserver agreement among endosonographers for the diagnosis of neoplastic versus non-neoplastic pancreatic cystic lesions," *Gastrointest. Endosc.* **58**(1), 59–64 (2003).
10. M. Pelaez-Luna and S. T. Chari, "Cyst fluid analysis to diagnose pancreatic cystic lesions: an as yet unfulfilled promise," *Gastroenterology* **130**(3), 1007–1009, discussion 1009 (2006).
11. B. G. Turner, S. Cizginer, D. Agarwal, J. Yang, M. B. Pitman, and W. R. Brugge, "Diagnosis of pancreatic neoplasia with EUS and FNA: a report of accuracy," *Gastrointest. Endosc.* **71**(1), 91–98 (2010).
12. M. B. Pitman, K. Lewandrowski, J. Shen, D. Sahani, W. Brugge, and C. Fernandez-del Castillo, "Pancreatic cysts: preoperative diagnosis and clinical management," *Cancer Cytopathol* **118**(1), 1–13 (2010).
13. P. J. Michaels, E. F. Brachtel, B. C. Bounds, W. R. Brugge, and M. Bishop Pitman, "Intraductal papillary mucinous neoplasm of the pancreas: cytologic features predict histologic grade," *Cancer* **108**(3), 163–173 (2006).
14. N. A. Belsley, M. B. Pitman, G. Y. Lauwers, W. R. Brugge, and V. Deshpande, "Serous cystadenoma of the pancreas: limitations and pitfalls of endoscopic ultrasound-guided fine-needle aspiration biopsy," *Cancer* **114**(2), 102–110 (2008).
15. P. L. Hsiung, D. R. Phatak, Y. Chen, A. D. Aguirre, J. G. Fujimoto, and J. L. Connolly, "Benign and malignant lesions in the human breast depicted with ultrahigh resolution and three-dimensional optical coherence tomography," *Radiology* **244**(3), 865–874 (2007).
16. D. Huang, E. A. Swanson, C. P. Lin, J. S. Schuman, W. G. Stinson, W. Chang, M. R. Hee, T. Flotte, K. Gregory, C. A. Puliafito, and J. Fujimoto, "Optical coherence tomography," *Science* **254**(5035), 1178–1181 (1991).
17. L. P. Hariri, G. T. Bonnema, K. Schmidt, A. M. Winkler, V. Korde, K. D. Hatch, J. R. Davis, M. A. Brewer, and J. K. Barton, "Laparoscopic optical coherence tomography imaging of human ovarian cancer," *Gynecol. Oncol.* **114**(2), 188–194 (2009).
18. M. Kraft, H. Glanz, S. von Gerlach, H. Wisweh, H. Lubatschowski, and C. Arens, "Clinical value of optical coherence tomography in laryngology," *Head Neck* **30**(12), 1628–1635 (2008).
19. R. A. McLaughlin, L. Scolaro, P. Robbins, S. Hamza, C. Saunders, and D. D. Sampson, "Imaging of human lymph nodes using optical coherence tomography: potential for staging cancer," *Cancer Res.* **70**(7), 2579–2584 (2010).
20. R. G. Michel, G. T. Kinasewitz, K. M. Fung, and J. I. Keddissi, "Optical coherence tomography as an adjunct to flexible bronchoscopy in the diagnosis of lung cancer: a pilot study," *Chest* **138**(4), 984–988 (2010).
21. J. A. Evans, B. E. Bouma, J. Bressner, M. Shishkov, G. Y. Lauwers, M. Mino-Kenudson, N. S. Nishioka, and G. J. Tearney, "Identifying intestinal metaplasia at the squamocolumnar junction by using optical coherence tomography," *Gastrointest. Endosc.* **65**(1), 50–56 (2007).
22. P. A. Testoni, A. Mariani, B. Mangiavillano, P. G. Arcidiacono, S. Di Pietro, and E. Masci, "Intraductal optical coherence tomography for investigating main pancreatic duct strictures," *Am. J. Gastroenterol.* **102**(2), 269–274 (2007).
23. R. Leitgeb, C. K. Hitzenberger, and A. F. Fercher, "Performance of Fourier domain vs. time domain optical coherence tomography," *Opt. Express* **11**(8), 889–894 (2003).
24. T. E. Ustun, N. V. Ifimtia, R. D. Ferguson, and D. X. Hammer, "Real-time processing for Fourier domain optical coherence tomography using a field programmable gate array," *Rev. Sci. Instrum.* **79**(11), 114301 (2008).
25. G. H. R. Zamboni and D. S. Longnecker, "Mucinous cystic neoplasms of the pancreas," in: S. R. Hamilton, L. A. Aaltonen, eds., *World Health Organization Classification of Tumours. Pathology and Genetics of Tumours of the Digestive System* (IARC Press, 2000).
26. B. C. Visser, B. M. Yeh, A. Qayyum, L. W. Way, C. E. McCulloch, and F. V. Coakley, "Characterization of cystic pancreatic masses: relative accuracy of CT and MRI," *AJR Am. J. Roentgenol.* **189**(3), 648–656 (2007).
27. B. Khurana, K. J. Mortelé, J. Glickman, S. G. Silverman, and P. R. Ros, "Macrocytic serous adenoma of the pancreas: radiologic-pathologic correlation," *AJR Am. J. Roentgenol.* **181**(1), 119–123 (2003).
28. M. Macari, M. E. Finn, G. L. Bennett, K. C. Cho, E. Newman, C. H. Hajdu, and J. S. Babb, "Differentiating pancreatic cystic neoplasms from pancreatic pseudocysts at MR imaging: value of perceived internal debris," *Radiology* **251**(1), 77–84 (2009).
29. J. S. Mallery, B. A. Centeno, P. F. Hahn, Y. Chang, A. L. Warshaw, and W. R. Brugge, "Pancreatic tissue sampling guided by EUS, CT/US, and surgery: a comparison of sensitivity and specificity," *Gastrointest. Endosc.* **56**(2), 218–224 (2002).
30. M. D'Onofrio, A. J. Megibow, N. Faccioli, R. Malagò, P. Capelli, M. Falconi, and R. P. Mucelli, "Comparison of contrast-enhanced sonography and MRI in displaying anatomic features of cystic pancreatic masses," *AJR Am. J. Roentgenol.* **189**(6), 1435–1442 (2007).
31. N. A. Ahmad, M. L. Kochman, J. D. Lewis, and G. G. Ginsberg, "Can EUS alone differentiate between malignant and benign cystic lesions of the pancreas?" *Am. J. Gastroenterol.* **96**(12), 3295–3300 (2001).

32. W. R. Brugge, K. Lewandrowski, E. Lee-Lewandrowski, B. A. Centeno, T. Szydlo, S. Regan, C. F. del Castillo, and A. L. Warshaw, "Diagnosis of pancreatic cystic neoplasms: a report of the cooperative pancreatic cyst study," *Gastroenterology* **126**(5), 1330–1336 (2004).
  33. S. Cizginer, V. Deshpande, N. Iftimia, C. Karaca, and W. R. Brugge, "Optical coherence tomography (OCT) imaging can detect fine morphologic features of pancreatic cystic neoplasms and differentiate between mucinous and non-mucinous cysts," *Gastroenterology* **136**(5), A-45 (2009).
- 

## 1. Introduction

Pancreatic cystic lesions represent an increasingly common diagnostic and therapeutic challenge [1]. A significant number of pancreatic cysts are detected incidentally when noninvasive abdominal imaging is performed for unrelated diagnosis [2]. The differentiation between low- and high-risk lesions is difficult with traditional imaging [3]. Low-risk lesions (simple cysts, pseudocysts, and serous cystadenomas [SCAs]) are generally not resected because they have no risk or an extremely low risk of malignant transformation [4]. High-risk lesions are mucin-producing tumors (mucinous cystic neoplasms [MCNs] and intraductal papillary mucinous neoplasms [IPMNs]) and cystic solid tumors (papillary cystic tumors, cystic ductal adenocarcinoma, and islet cell tumor) [5]. Depending on degree of dysplasia [6], MCNs and IPMNs are classified as adenoma, borderline, carcinoma in situ, or invasive cancer.

An accurate diagnosis of a pancreatic cystic lesion is often difficult because traditional cross-sectional imaging tests cannot provide diagnostic resolution images [7]. Traditionally, computed tomography (CT) has been used as a first line of diagnosis for cystic neoplastic lesions of the pancreas. However, the limited resolution of CT scanning prevents reliable differentiation of the pancreatic cysts [8]. More recently endoscopic ultrasound (EUS) has been used to image the pancreas with improved resolution. Because the pancreas lies directly adjacent to the stomach, an EUS transducer can be placed in close proximity to the pancreas, and the entire gland can be readily imaged. Although EUS is well suited for assessment of cystic lesions because it can provide images of the cystic wall and septations, it has not been able to accurately differentiate between benign and malignant cystic neoplasms [9]. Either of these techniques can be supplemented by the use of fine needle aspiration (FNA) cytology for diagnostic yield enhancement. However, the results of cyst fluid analysis have been somewhat disappointing [10]. Although EUS-guided FNA of pancreatic masses is a highly sensitive test for diagnosing pancreatic malignancy, the results of FNA of pancreatic cysts have not been as successful [11]. Obtaining sufficient cells for diagnostic cytology is often difficult because of the relatively low cellularity of aspirated pancreatic cyst fluid [12–14]. Therefore, the accuracy of EUS-FNA can still vary over a relatively large range (69% to 100%).

Recently, optical coherence tomography (OCT), a high resolution structural imaging technology based on low coherence interferometry, has shown great promise in disease diagnosis, including differentiation between benign and malignant lesions [15]. OCT is an interferometric technique, typically employing near-infrared light, and allows for achieving micron-scale cross-sectional images of the biological samples [16]. The use of relatively long wavelength light allows it to penetrate up to 2 mm into a highly scattering media, such as biological samples. OCT images are somewhat similar to those provided by conventional ultrasound, but OCT provides at least one order of magnitude increase in the resolution. However, the main drawback of this technology is that its field of view is limited to several mm.

OCT studies in various organs have demonstrated the ability of OCT to differentiate between normal and pre-malignant conditions. For example, ovarian cysts, masses, and abnormal tissue have been successfully imaged with laparoscopic OCT [17]. Laryngeal dysplasia and malignancy have been successfully imaged with OCT probes during laryngoscopy [18]. Malignant and inflammatory lymph nodes have been differentiated with OCT [19]. Early investigations using bronchoscopic OCT probes have also demonstrated the ability of OCT to diagnose lung cancer [20]. Intestinal metaplasia and dysplastic Barrett's

esophagus have been evidenced with endoscopic OCT [21]. Early investigations of OCT in the pancreas have also demonstrated the ability of this technology to distinguish the layers of the main duct epithelium in inflammatory and malignant diseases [22].

This paper presents the results of a pilot study that had the goal to investigate the possibility of using OCT imaging for differentiating between morphologic features of low risk pancreatic cysts (i.e. pseudocysts and SCAs) and high risk pancreatic cysts (i.e., MCNs and IPMNs). We hypothesized that OCT imaging could be used to more reliably differentiate between two classes of pancreatic cysts: mucinous and serous.

## 2. Materials and Methods

### 2.1 OCT Instrumentation

An OCT system based on the Fourier domain approach [23], developed by Physical Sciences, Inc. (PSI), was used for this study. A simplified schematic and a photograph of this instrument are shown in Fig. 1. It uses a swept-source (Model HSL-1000, SANTEC, Japan) with a central wavelength of 1310 nm, a bandwidth of about 89 nm, and a scanning frequency of 20 kHz. The light from the swept source is sent to a fiber optic interferometer that uses a circulator in the input arm to maximize the amount of light that is transmitted to the sample and also the amount of light reflected back from the sample. A fraction of the light backscattered from the sample passes back through the probe into the interferometer, where it mixes with a reference beam to produce interference fringes. A balanced detection scheme is used in the detection arm of the interferometer. Balanced detection helps to minimize the intensity noise of the light source. The balanced detector (Model 1817FC, New Focus) has a bandwidth of 80 MHz and a  $5 \times 10^4$  V/A transimpedance gain of  $5 \times 10^4$  V/A. The output of the detector is digitized with a PSI custom-made high-speed and very low noise digitizer (50 Megasamples/sec digitization rate). The signal at the output of the digitizer is sent to a custom real-time digital signal processing (DSP) board, also custom-designed and fabricated by PSI, which performs the fast Fourier transform of the signal to obtain the depth reflectivity profile of the sample. Detailed description of the digitization and signal processing boards was presented elsewhere [24]. A LabView-based software program is used for displaying the processed OCT images on the computer screen and for configuring the real time board.

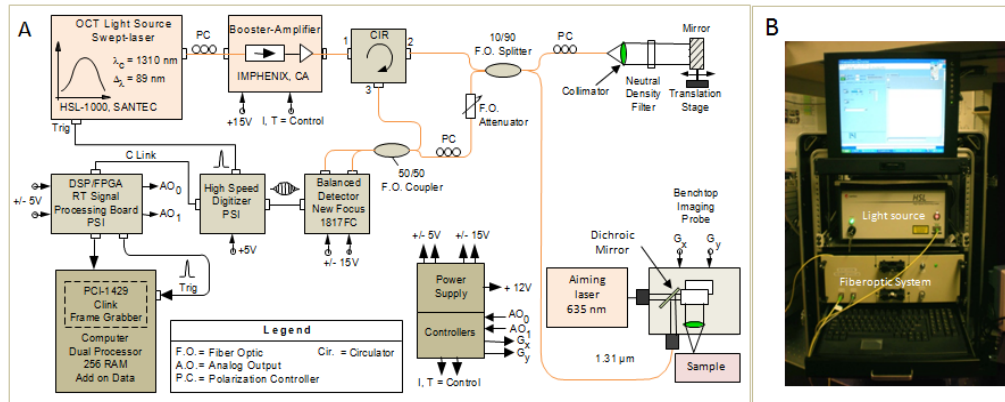


Fig. 1. Simplified schematic (A) and photograph of the OCT system (B).

The OCT system was integrated within a 19 inch wheeled rack, which allowed for easy rolling in and out of the imaging room of the hospital. A benchtop OCT probe was used to image the surface of the cyst. The OCT probe had an OCT port and a laser port, as shown in the schematic from Fig. 1. The laser port was used to send a visible aiming beam (635 nm) and visualize the position of the near-infrared OCT beam on the tissue surface. The bench-top imaging probe also contained a pair of galvanometers, which allowed for generating a raster

scan, a custom filter that was used to combine the 1310 nm and 635 nm beams, and an objective scan lens (LSM03, Thorlabs, NJ). This system provided an axial resolution of 9.5  $\mu\text{m}$  (in air), which is close to the theoretical value of 8.5  $\mu\text{m}$ , and a lateral resolution of 25  $\mu\text{m}$ . A scanning range of maximum 5 mm was used on both dimensions with this probe. Each OCT frame (B-scan) contained 1024 A-lines, while each raster (C-scan) contained 256 frames.

## 2.2 OCT Imaging of Tissue Specimens

A human protocol for this study was approved by the MGH Human Research Committee to analyze the correlation between the OCT images and the histologic appearance of the pancreatic surgical specimens from patients who had a surgical resection at the Massachusetts General Hospital. No patient identifiers were provided to the investigators of this study.

Fresh pancreatic tissue specimens (pancreatic cysts) were made available immediately after surgery. The cysts were transected along the long axis to fully expose the luminal surface. The cystic tissue was then placed on a Petri dish in a saline bath to keep it moist. A pair of linear positioning stages was used for proper positioning of the tissue specimen under the OCT imaging objective. For correct imaging-histology co-registration, a visible-light guiding-beam (635-nm laser diode) that was coincident with the near-infrared interrogating OCT beam was used. The targeted imaging site of the cyst epithelium surface was labeled with India ink in order to perform histopathology correlation with the OCT findings. OCT tomography imaging of India ink labeled cyst surface was performed to test OCT capability for revealing the detailed anatomy of cystic wall, as well as of the cyst fluid. Representative OCT images of the tissue morphology were collected and saved for later histopathologic correlation.

## 2.3 Histopathologic Examination

After completion of the OCT examination, the specimens were fixed with 10% formalin and embedded in paraffin. Tissue sections were then obtained and stained with hematoxylin and eosin for routine histopathologic examination. The histopathologic diagnostic criteria of pancreatic cysts were based on the World Health Organization classification system [25]. All sections were examined and characteristic histopathologic findings were noted independently by an experienced GI pathologist blinded to the OCT findings.

## 2.4 Data Analysis

Based on histology results, the cysts were prospectively divided into two groups, mucinous (MCNs and IPMNs) and non-mucinous (SCAs and others). The initial analysis of OCT and histology results was performed by independent investigators, blinded to each other's findings. A training set of 20 specimens, representative for both mucinous and non-mucinous lesions were selected by the study coordinator (SC) and OCT-histology correlation was performed. The characteristic OCT features for each type of pancreatic cystic lesions from the training set were standardized and defined as "OCT criteria" for differentiation of cystic lesions. The remaining set of 46 tissue specimens was then attributed to the validation study. The standard OCT criteria were prospectively applied to OCT images from this set by three clinicians blinded to histopathological findings. The clinicians were asked to assign each OCT image to one of four different categories: 'MCN', 'IPMN', 'SCA', and 'other'. After that, correlation with histology results was performed. Out of the total 46 samples, 26 were found to be serous after histologic examination, while the remaining 20 were found to be mucinous.

All data were entered and stored in a computerized database designed with Microsoft Excel 2000. Specificity, sensitivity, and accuracy were calculated for each observer. The histology was used as the 'gold' standard for classifying the cysts into two groups, mucinous and non-mucinous. The sensitivity and the specificity of the findings were calculated using the following formulas: Sensitivity =  $TP/(TP + FN)$ ; Specificity =  $TN/(TN + FP)$ . True

positive (TP) interpretation reflected the accurate diagnosis of a mucinous lesion by OCT, while true negative (TN) interpretation reflected the accurate diagnosis of a non-mucinous lesion. False positive (FP) reflected incorrectly identified mucinous lesions, while false negative (FN) reflected incorrectly identified serous lesions. The Positive and Negative Predictive values were calculated as well using the following formulas:  $PPV = TP/(TP + FP)$ ;  $NPV = TN/(TN + FN)$ .

Inter-observer agreement of overall OCT prediction for differentiation of cystic lesions among the three readers and agreement between the overall OCT diagnosis and histopathologic type (for the three readers) were studied using the kappa statistic. Kappa statistical results were classified as follows: less than chance agreement (<0), slight agreement (0.01-0.2), fair agreement (0.21-0.4), moderate agreement (0.41-0.6), substantial agreement (0.61-0.8), and almost perfect agreement (0.81-0.99).

### 3. Results

The OCT images of each tissue specimen were correlated with histological findings by identifying India ink marks, as well as notable and unique features of each tissue type.

The OCT images of most of the microcystic SCAs were remarkably similar and all demonstrated multiple tiny cysts with well-defined outlines (Fig. 2(A)). The thin septae between the cysts showed homogeneously high scattering, creating a honeycomb appearance. Significantly, the cyst contents were homogeneously dark and lacked scattering effect. Histologically, this appearance correlated with the microcystic appearance of a serous cystadenoma (Fig. 2(A')). In a single case, focal intraluminal scattering was noted on OCT (Fig. 2(B)), and this corresponded to a focus of fresh intraluminal hemorrhage shown in the histological appearance (Fig. 2(B')).

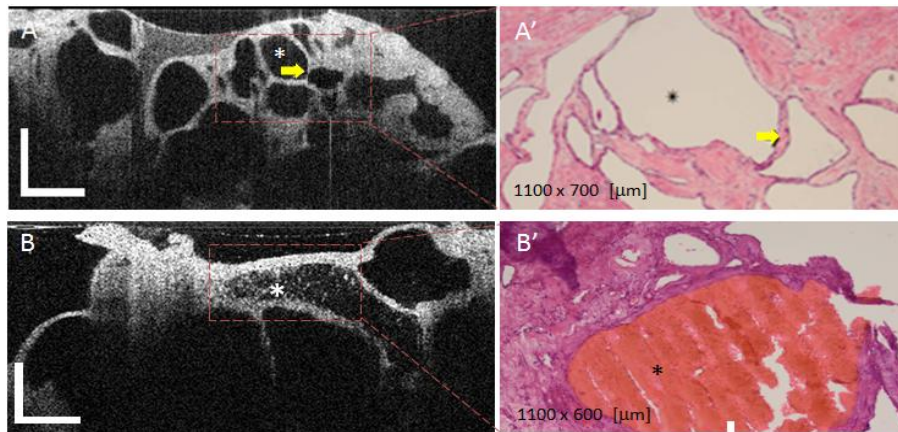


Fig. 2. OCT appearance of SCAs (A) and (B) and corresponding histology (A', B'). The microcystic SCAs show multiple tiny cysts with well-defined outlines. The thin septae between the cysts (see arrow), creating a honeycomb appearance, shows homogeneously high scattering. The cyst content usually lacks a scattering effect. Focal intraluminal scattering can be noted on some cysts (see asterisk in Fig. 2(B)) and it usually corresponds to a focus of intraluminal hemorrhage, as confirmed by histology (see red area Fig. 2(B')). OCT scale bar = 500  $\mu$ m.

Raster scans of these cysts were taken as well to determine their 3D appearance. An example of a scan through a typical microcystic SCA is shown in the [Media 1](#). Two representative slides (*enface* and cross-sectional) of this benign cyst are shown in Fig. 3. The *enface* view is shown on the left side of Fig. 3, while a perpendicular cross-section in the position indicated by the line from the *enface* view is shown on the right side of Fig. 3. Both views show the thin septae between the microcysts, which creates a honeycomb appearance.

In addition, excepting some hemorrhagic microcysts, the microcystic content is homogeneously dark due to lack of scattering structures (clear fluid).

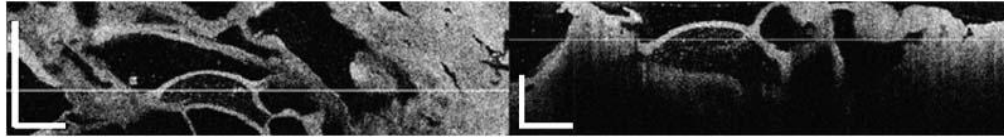


Fig. 3. (Media 1). Fly-through video of a SCA. (A) *Enface* view at a depth indicated by the line from the cross-sectional image. (B) cross-sectional view. The raw video was acquired at 20 fps. Scale bar = 500  $\mu\text{m}$ .

The OCT images of MCNs (Fig. 4) demonstrated several 'daughter' cysts (see yellow arrow) within the rind of tissue surrounding the dominant unilocular cyst (see red arrow). Unlike SCAs, there was high scattering within the lumen of these cysts, and on histology this appearance corresponded to intraluminal mucin (Fig. 3 right). Furthermore, unlike SCAs, these cysts were separated by large amount of homogenous high scattering tissue that corresponded to the intervening fibrocollagenous tissue.

Raster scans of these cysts were also taken to visualize their 3D appearance. An example of a scan through a typical MCN is shown in the Media 2. Two representative slides (*enface* and cross-sectional) of this potentially malignant cyst are shown in Fig. 5. The *enface* view is shown on the left side of Fig. 5, while a perpendicular cross-section in the position indicated by the line from the *enface* view is shown on the right side of Fig. 5. Both views show the presence of the thicker microcystic wall than in the SCA case and a highly scattering fluid (mucin). The scattering is thought to come by the presence of the dead exfoliating cells from the thick cystic epithelium.

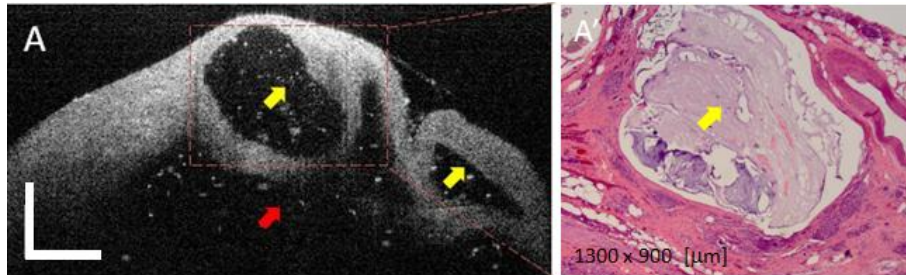


Fig. 4. OCT appearance of a mucinous cyst (A) and corresponding histology (B). Yellow arrows indicate the presence of smaller size (daughter) cysts, while the red arrow indicates the main cystic cavity. The cystic content (mucin) shows some scattering due the presence of dead epithelial cells. OCT scale bar = 500  $\mu\text{m}$ .



Fig. 5. (Media 2). Fly-through video of a MCN. (A) *Enface* view at a depth indicated by the line from the cross-sectional view. (B) Cross-sectional view. The raw video was acquired at 20 fps. Scale bar = 500  $\mu\text{m}$ .

The OCT images of IPMNs (Fig. 6(A)) were similar to those of MCNs in that they demonstrated multiple cysts with heterogeneous intraluminal medium to high scattering that corresponded to mucin content seen in the histological appearance (Fig. 6(B')). However, the cysts were smaller in size and large unilocular cysts were not found.

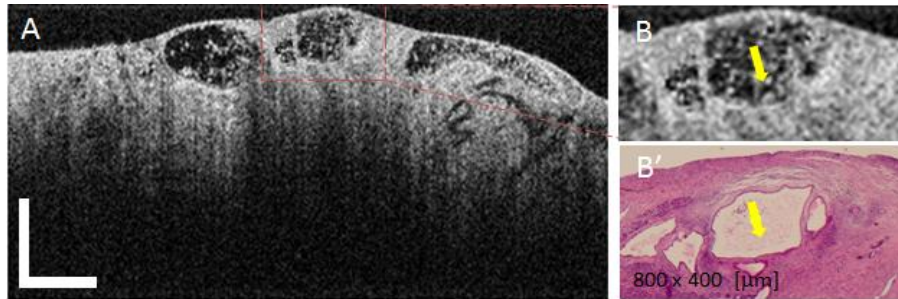


Fig. 6. OCT appearance of mucinous IPMN cysts (A), magnified ROI (B), and corresponding histology (B'). Yellow arrows indicate the areas of highly scattering mucin within the cyst fluid. OCT Scale bar = 500  $\mu\text{m}$ .

Raster scans were taken as well for these cysts. An example of a scan through a typical IPMN is shown in the [Media 3](#). Two representative slides (*enface* and cross-sectional) of this potentially malignant cyst are shown in Fig. 7. The *enface* view (on the left) was taken at a depth indicated by a line in the vertical cross-section (on the right). The line in the *enface* image shows the position where the perpendicular cross-sectional image was taken. Both views show the presence small size microcysts, very close to the cyst surface. The microcysts are separated by larger amounts of tissue than in the case of microcystic SCAs. The microcysts contain a highly scattering fluid, similar to MCNs.

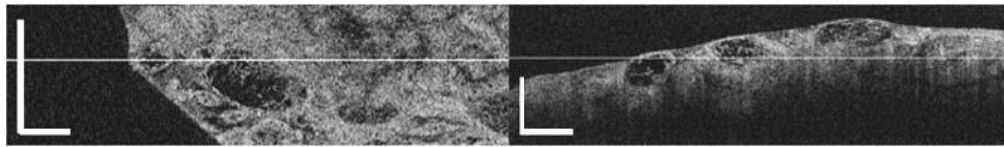


Fig. 7. ([Media 3](#)). Fly-through video of a IPMN. (A) *Enface* view. (B) Cross-sectional view. The raw video was acquired at 20 fps. Scale bar = 500  $\mu\text{m}$ .

OCT criteria for differentiating between MCNs, SCAs, and IPMNs were developed using OCT images from representative cystic lesions from a set of 20 tissue samples (training set), which were selected by the histopathologist. The main characteristics of each type of cystic lesion are shown in Fig. 8. As it can be observed, these criteria are mainly based on the visual appearance of the cystic wall morphology and on the scattering properties of the cystic fluid. Although relatively simple, they provided a very good discrimination between serous and mucinous cysts. Based on these criteria, randomly selected OCT images of the 46 tissue specimens (validation set) were independently evaluated by a gastroenterologist, a radiologist and a pathologist. The investigators were asked to review each OCT image and assign the image to one of 4 categories (MCN, IPMN, SCN, other). OCT results were judged against histopathology findings. Using histology as the ‘gold’ standard for correctly diagnosing each type of cyst, the rates of sensitivity, specificity were determined for OCT.

The summary of the OCT-histology correlation analysis is shown in Table 1. High sensitivities (95.6% for gastroenterologist and 100% for radiologist and pathologist) were obtained for distinguishing between mucinous and non-mucinous cystic lesions. However, of these successfully distinguished mucinous cystic lesions, only the radiologist accurately (100% sensitivity and 85% specificity) distinguished IPMNs from MCNs. Nevertheless, all three physicians were moderately successful identifying MCNs with a specificity of 85% for the radiologist and 92% for both the gastroenterologist and pathologist.



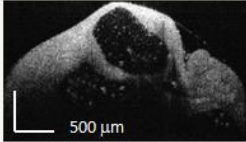
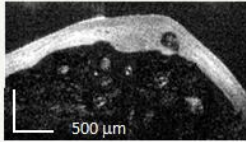
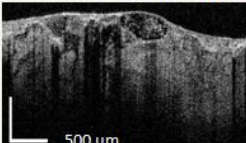
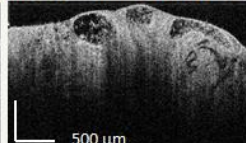
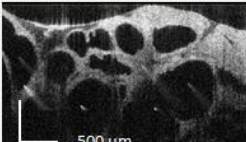
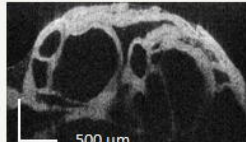
OCT Image		Specific OCT Features
<b>Mucinous Cystic Neoplasms</b>		
		<ul style="list-style-type: none"> <li>• Large cavity cysts (over several mm in size, see red arrow area), sometimes surrounded by multiple relatively small diameter microcysts (higher than several hundred <math>\mu\text{m}</math> in size, see yellow arrow)</li> <li>• Well defined thick mural layer</li> <li>• Moderate to high scattering in the lumen</li> </ul>
<b>Intraductal Papillary Mucinous Neoplasms</b>		
		<ul style="list-style-type: none"> <li>• Multilocular small cysts (less than 500 <math>\mu\text{m}</math> in size)</li> <li>• Moderate to high scattering in the lumen</li> <li>• Well defined thick mural layer</li> <li>• Located within or very close to the pancreatic duct</li> </ul>
<b>Serous Cyst Adenomas</b>		
		<ul style="list-style-type: none"> <li>• Multiple small cysts separated by a delicate septae</li> <li>• Cystic lumen not larger than 2 mm</li> <li>• Honeycomb appearance</li> <li>• Clear-lack of OCT signal in the lumen</li> </ul>

Fig. 8. OCT diagnostic criteria for pancreatic cysts.

Kappa statistics, also presented in Table 1, suggest that all three physicians exhibited “almost perfect” overall agreement in distinguishing mucinous cystic lesions with kappa = 0.95 between radiologist and gastroenterologist agreement, and kappa = 0.95 between radiologist and pathologist agreement. Agreement between gastroenterologist and pathologist was slightly lower with a kappa statistic of 0.91.

Table 1. Sensitivity, Specificity, and Kappa Analysis

SENSITIVITY AND SPECIFICITY ANALYSIS			
Mucinous vs. Non-mucinous			
Reviewer	Gastroenterologist	Radiologist	Pathologist
Sensitivity(%)	95.6 (78, 100)	100 (85, 100)	100 (85, 100)
Specificity (%)	100 (85, 100)	100 (85, 100)	95.6 (78, 100)
Negative Predictive Value (%)	95.8 (79, 100)	100 (85, 100)	100 (85, 100)
Positive Predictive Value (%)	100 (85, 100)	100 (85, 100)	95.8 (79, 100)
IPMNs vs. MCNs			
Sensitivity(%)	50 (19, 81)	100 (69, 100)	30 (0.07, 65)
Specificity (%)	92 (62, 100)	85 (55, 98)	92(64, 100)
Negative Predictive Value (%)	83 (36, 100)	83 52, 98)	75 (19, 99)
Positive Predictive Value (%)	69 (41, 89)	100 (72, 100)	63 (38, 84)
KAPPA ANALYSIS			
	Kappa	95% LCL (Lower Confidence Limit)	95% UCL (Upper Confidence Limit)
Radiologist x Gastroenterologist	0.957	0.872	1.000
Gastroenterologist x Pathologist	0.913	0.796	1.000
Radiologist x Pathologist	0.957	0.872	1.000

#### 4. Discussion and Conclusions

The detection of pancreatic cystic lesions by cross sectional CT or MR imaging is dependent on the identification of a low attenuation area within the pancreas. CT and MRI are both

highly sensitive to such lesions. However, the differentiation between various types of cysts is difficult with either imaging modality. Despite major advances in imaging, the overall accuracy of cross sectional imaging for pancreatic cysts diagnosis remains rather low [26]. An accurate CT diagnosis is hampered by poor resolution of septation patterns (macro and microcystic morphology) [27,28]. In addition, nearly 20% of cysts that are classified based on septation pattern are inaccurately diagnosed because of a large overlap between the macrocystic and microcystic morphology among both mucinous and non-mucinous cysts [28]. Endoscopic ultrasound (EUS) imaging provides superior accuracy compared to CT. In addition to enhanced resolution, it takes advantage of the close proximity of the ultrasound transducer to the pancreas. Therefore, ultrasound is more sensitive than CT and MRI in the detection of intracystic septations [29,30]. Nevertheless, EUS imaging alone still has a relatively low diagnostic rate in the differentiation of various cyst types [31]. The use of EUS-FNA aspiration for fluid collection has enabled endoscopists to use the presence of tumor markers and abnormal cytology to supplement EUS imaging [11]. Despite these advances, the accuracy of EUS and cyst fluid analysis for the differentiation between mucinous and non-mucinous cysts still remains modest [14,31,32].

We have evaluated the use of a high resolution OCT imaging in the diagnosis of pancreatic cystic lesions. In our study, we performed *ex vivo* pancreatic imaging using a benchtop probe. Since previous OCT studies in various organs demonstrated the ability of OCT to differentiate between normal and pre-malignant conditions [17–21], we hypothesized that OCT might also be able to differentiate between the interior structures of various pancreatic cystic lesions. Early investigations of OCT in the pancreas have also demonstrated the ability of this technology to distinguish the layers of the main duct epithelium in inflammatory and malignant diseases [22].

We have recently reported OCT use for imaging morphologic features of pancreatic cysts [33]. Similar to the methods used for the imaging of the intestinal metaplasia and dysplasia seen in Barrett's esophagus, we have placed a high resolution probe directly adjacent to the cut surface of the pancreatic cysts. Using a wide variety of pancreatic cysts, we were able to demonstrate excellent correlations between OCT images and the histologic features of serous cysts and microcystic septations. Along similar lines, we were able to provide some key imaging features of the mucinous cystic lesions, for example, the high scattering of the mucinous fluid and the presence of a large amount of homogenous high scattering tissue between the microcysts that corresponds to the intervening fibrocollagenous tissue the increased epithelial thickness of the malignant cysts. We found strong correlations between histology and OCT imaging in a learning set of images from twenty tissue specimens. In our initial phase of testing, we examined the accuracy and the correlation of OCT imaging with the histological appearance of the cysts based on an unblinded analysis. Based on the experience obtained with the learning set of OCT images, we proceeded with a blinded analysis of OCT images by three different clinicians. The cysts were determined to be mucinous or non-mucinous based on pre-established OCT criteria and the results were compared with histology findings. Despite modest training and little experience with OCT imaging, the three clinicians were able to identify mucinous cysts with high levels of accuracy (96-100%). Furthermore, there was very good consistency as demonstrated with Kappa statistics.

Our preliminary study was limited to *ex vivo* imaging and had the goal of investigating the use of OCT imaging for differentiating between serous and mucinous pancreatic cysts. Cystic wall morphology and scattering of the cystic fluid were the main features used for cyst differentiation. However, additional features, like the thickness of the cystic epithelium could be used as well to determine the malignancy potential of the mucinous cysts or to aid in differentiating between serous and mucinous cysts. For example, a very difficult problem for the gastroenterologist is to differentiate between low grade and high grade MCNs/IPMNs. It is known from histological examination that high grade mucinous cysts have substantially

increased epithelial thickness (over 20  $\mu\text{m}$ ). By contrary, SCAs have an epithelial thickness lower than 10  $\mu\text{m}$ , and the epithelium does not suffer severe modifications while the cyst continues to grow. Unfortunately, the limited resolution of the OCT system did not provide very reliable differentiation between the two main categories of analyzed cysts based on epithelial thickness. Therefore, we have recently built another OCT system and endoscopic probe that will provide enhanced axial and lateral resolution (8  $\mu\text{m}$ , and 20  $\mu\text{m}$  respectively), and thus might help to include epithelial features in our criteria for cystic lesions differentiation.

Besides imaging resolution, imaging range and penetration depth are two important parameters that also need further attention. Unfortunately, the penetration depth for OCT is generally limited to about 2 mm, and thus only a small area of the cystic lesion can be evaluated at the time, for a given position of the OCT probe within the cyst. Therefore, *in vivo* imaging will require OCT probe positioning in several different areas of the cyst to get a more complete picture of cyst morphology. With regard to the imaging range, it is desirable to investigate larger areas of cystic microcavities for a given localization of the OCT probe within the cyst. This is especially important for MCNs, which can have small size (hundreds of microns) daughter microcysts (microcavities), but also larger cavities on the order of tens of millimeters. However, although the imaging range of the OCT system can be made within the order of 6 to 12 mm, the potential of imaging large cavities is limited by the relatively short working distance of the OCT probe. This parameter cannot be made too large (over 2–3 mm) without compromising imaging lateral resolution, unless a dynamic focusing scheme is implemented. Therefore, we will further investigate various design approaches for the OCT probe before moving to an *in vivo* study.

In summary, OCT provided high resolution images of the cyst morphology, enabling clinicians to accurately differentiate between serous and mucinous cysts. Although imaging was performed in an *ex vivo* setting, our results suggest that there is a good likelihood that intra-cystic OCT imaging with a minimally invasive probe would also allow for reliable differentiation between serous and mucinous cysts. These findings are important because of the potential of OCT imaging to supplement the results of EUS. We are currently planning to perform a pilot *in vivo* study to further explore the potential of OCT imaging for aiding EUS-FNA in differentiating between various cystic lesions of the pancreas.